Elsevier Editorial System(tm) for Earth and Planetary Science Letters
Manuscript Draft

Manuscript Number: EPSL-D-13-01232R1

Title: The H2O content of granite embryos

Article Type: Letters

Keywords: nanogranite; NanoSIMS; melt inclusions; granite H2O content; crustal melting; granite embryos

Corresponding Author: Dr. Omar Bartoli,

Corresponding Author's Institution: University of Padova

First Author: Omar Bartoli

Order of Authors: Omar Bartoli; Bernardo Cesare; Laurent Remusat; Antonio Acosta-Vigil; Stefano Poli

Abstract: Quantification of H2O contents of natural granites has been an on-going challenge owing to the extremely fugitive character of H2O during cooling and ascent of melts and magmas. Here we approach this problem by studying granites in their source region (i.e. the partially melted continental crust) and we present the first NanoSIMS analyses of (remelted) nanogranites. Nanogranites are crystallized melt inclusions (MI) hosted in peritectic phases of anatectic rocks and represent the embryos of the upper-crustal granites. The novel approach based on the combination of nanogranites and NanoSIMS has been here tested on amphibolite-facies migmatites at Ronda (S Spain) that underwent fluid-present to fluid-absent melting at ~700 °C and ~5 kbar. Nanogranites trapped in garnet have been remelted using a piston-cylinder apparatus. We measure high and variable H2O contents (mean of 6.5±1.4 wt%) in these low-temperature, low-pressure granitic melts. We demonstrate that, when the entire population from the same host is considered, MI reveal the H2O content of melt in the specific volume of rock where the host garnet grew. Mean H2O values for the MI in different host crystals range from 5.4 to 9.1 wt%. This range is in rather good agreement with experimental models for granitic melts at the inferred P-T conditions. Our study provides a well-characterized snapshot of the partially melted natural continental crust, in particular of the onset of anatexis, and documents for the first time the occurrence of H2O heterogeneities in granitic melts at the source region. These heterogeneities are interpreted to reflect the birth of granitic melts under conditions of "mosaic" equilibrium, where the distinct fractions of melt experience different buffering assemblages at the micro-scale, with concomitant differences in melt H2O content. These results confirm the need for small-scale geochemical studies on natural samples to improve our quantitative understanding of crustal melting and granite formation. The same novel approach adopted here can be successfully applied to nanogranites hosted in higher-temperature, granulite-facies rocks that represent the parents of many upper-crustal granites.

The H_2O content of granite embryos

Omar Bartoli[a*], Bernardo Cesare[a], Laurent Remusat[b], Antonio Acosta-Vigil[c], Stefano Poli[d]

[a]*Dipartimento di Geoscienze, Università di Padova, Via Gradenigo 6, 35131 Padova, Italy*
[b]*Muséum National d'Histoire Naturelle, Laboratoire de Minéralogie et Cosmochimie du Muséum (LMCM), 61, rue Buffon, 75005 Paris, France*
[c]*Instituto Andaluz de Ciencias de la Tierra, Consejo Superior de Investigaciones Científicas-Universidad de Granada, Avda. de Las Palmeras nº 4, Armilla 18100, Granada, Spain*
[d]*Dipartimento di Scienze della Terra, Università di Milano, Via Botticelli 23, 20133 Milano, Italy*

*Corresponding author: Dipartimento di Geoscienze, Università di Padova, Via Gradenigo 6, 35131 Padova, Italy.
Phone: +39 339 3667870
E-mail: omar.bartoli@unipd.it

ABSTRACT

Quantification of H_2O contents of natural granites has been an on-going challenge owing to the extremely fugitive character of H_2O during cooling and ascent of melts and magmas. Here we approach this problem by studying granites in their source region (i.e. the partially melted continental crust) and we present the first NanoSIMS analyses of (remelted) nanogranites. Nanogranites are crystallized melt inclusions (MI) hosted in peritectic phases of anatectic rocks and represent the embryos of the upper-crustal granites. The novel approach based on the combination of nanogranites and NanoSIMS has been here tested on amphibolite-facies migmatites at Ronda (S Spain) that underwent fluid-present to fluid-absent melting at ~700 °C and ~5 kbar. Nanogranites trapped in garnet have been remelted using a piston-cylinder apparatus. We measure high and variable H_2O contents (mean of 6.5±1.4 wt%) in these low-temperature, low-pressure granitic melts. We demonstrate that, when the entire population from the same host is considered, MI reveal the H_2O content of melt in the specific volume of rock where the host garnet grew. Mean H_2O values for the MI in different host crystals range from 5.4 to 9.1 wt%. This range is in rather good agreement with experimental models for granitic melts at the inferred P-T conditions. Our study provides a well-characterized snapshot of the partially melted natural continental crust, in particular of the onset of anatexis, and documents for the first time the occurrence of H_2O heterogeneities in granitic melts at the source region. These heterogeneities are interpreted to reflect the birth of granitic melts under conditions of "mosaic" equilibrium, where the distinct fractions of melt experience different buffering assemblages at the micro-scale, with concomitant differences in melt H_2O content. These results confirm the need for small-scale geochemical studies on natural samples to improve our quantitative understanding of crustal melting and granite formation. The same novel approach adopted

here can be successfully applied to nanogranites hosted in higher-temperature, granulite-facies rocks that represent the parents of many upper-crustal granites.

Key words: nanogranite ; NanoSIMS; melt inclusions; granite H_2O content; crustal melting; granite embryos

Research highlights:

- First time in literature of NanoSIMS applied on nanogranite inclusions;
- H_2O content of embryos of the upper-crustal anatectic granites;
- Mean H_2O values for the selected host crystals between 5.4 and 9.1 wt%;
- H_2O content heterogeneities of granitic melts at the source region

1. Introduction

The formation, extraction and ascent of hydrous granitic melts and magmas to upper crustal levels represent the most important mechanisms for the reworking of the Earth's continental crust (Brown et al., 2011; Sawyer et al., 2011; Vielzeuf et al., 1990). In this scenario, the H_2O content of melts and magmas is of prime relevance in the formation and evolution of granites, as recognized by the pioneering works of Goranson (1931) and Tuttle and Bowen (1958). For these reasons, Campbell and Taylor (1983) stated, "*Water is essential for the formation of granite and granite, in turn, is essential for the formation of continents. Earth, the only inner planet with abundant water, is the only planet with granite and continents*". As a matter of fact, the influence of H_2O on the chemical and physical properties of granitic (s.l.) magmas has a long history of investigation (e.g., Burnham, 1967, 1975; Burnham and Ohmoto, 1980; Clemens and Vielzeuf, 1987; Dingwell, 1987; Keppler, 1989; Kushiro, 1978; Scaillet et al., 1996; Shaw, 1963).

Despite all these critical phenomena, H_2O quantification in natural granitic systems remains an on-going challenge in granite petrology. The primary difficulty stems from H_2O exsolution and diffusion from granitic melts and magmas during cooling and ascent (e.g., Burnham, 1967; Candela, 1997; White and Powell, 2010). Moreover, crustal granites may not represent pure melts (e.g., Clemens and Stevens, 2012; Stevens et al., 2007). Clemens (1984), reviewing different approaches to quantify the H_2O content of silicic to intermediate magmas at that time, concluded that the most promising methods for crystalline rocks were the experimental approaches. Accordingly, in the last decades a phase equilibria-based experimental approach has been largely applied to obtain constraints on the H_2O content of granites (e.g., Clemens et al., 1986; Clemens and Wall, 1981; Dall'Agnol et al., 1999; Holtz et al., 2001; Maaløe and Wyllie, 1975; Scaillet et al., 1995).

On the other hand, the huge amount of experimental works performed since the 80's to investigate the melting of natural metapelites and metagreywackes or synthetic mixtures (e.g. Carrington and Harley, 1995; Holtz and Johannes, 1991; Icenhower and London, 1995; Le Breton and Thompson, 1988; Montel and Vielzeuf, 1994, 1997; Patiño-Douce and Beard, 1995; Patiño-Douce and Harris, 1998; Patiño-Douce and Johnston, 1991; Spicer et al., 2004; Stevens et al., 1997; Vielzeuf and Holloway, 1988; Ward et al., 2008) has suffered from the lack of proper analytical tools for measuring directly the H_2O content of quenched granitic glasses.

Recently, a comprehensive database on H_2O contents of granitic magmas has been compiled using melt inclusions (MI) hosted in minerals of granite, mostly quartz and topaz (Thomas and Davidson, 2012). This approach is totally based on natural occurrences (i.e. MI in granite) and has provided information largely ignored before. The frequency diagram of the H_2O content measured in granite MI provided three maxima at 4.0, 5.9 and 8.1 wt% which have been related to different stages of magma evolution (Thomas and Davidson, 2012). Indeed, MI in granites are representative of evolved, and sometimes highly fractionated, magmas (Thomas and Davidson, 2012; Webster and Rebbert, 2001; Webster and Thomas, 2006) and, therefore, they are considered not to be useful for discussing the initial conditions of formation of granitic magmas (Clemens and Watkins, 2001).

Large volumes of granitic melts are widely thought to form by incongruent melting reactions (Clemens and Vielzeuf, 1987; Clemens and Watkins, 2001; Sawyer et al., 2011). Such reactions produce peritectic solid phases that may trap droplets of melt –i.e. MI– produced simultaneously (Cesare et al., 2009; Darling, 2013; Ferrero et al., 2012). Upon slow cooling, these MI generally crystallize to cryptocrystalline aggregates named "nanogranites" (Cesare et al., 2009). To obtain the composition of trapped melts,

nanogranite inclusions must be remelted to a homogeneous liquid (Bartoli et al., 2013b). More rarely, in some exceptional geological contexts such as anatectic enclaves hosted in lavas, melt can be quenched to glass during eruption of the host volcanic rocks (Acosta-Vigil et al., 2007; Cesare et al., 1997, 2003; Di Martino et al., 2011; Ferrero et al., 2011; Frezzotti et al., 2004). Because nanogranite and glassy MI hosted in peritectic phases of anatectic rocks correspond to the first batches of melt, whose subsequent segregation, redistribution, ascent and accumulation out of the source regions result in the formation of granitic bodies at shallow crustal levels (Brown, 2013; Brown et al., 2011), they represent the embryos of the upper-crustal anatectic granites and may provide a wealth of information on granite genesis (Acosta-Vigil et al., 2010, 2012a; Bartoli et al., 2013b). However, the accurate compositional characterization of these recently discovered, small data repositories is still challenging owing to their size (commonly < 15 µm; see Bartoli et al., 2013a; Ferrero et al., 2012), which is close, or below, the limits of resolution of conventional analytical techniques.

Here we make use of considerable advances in secondary ion mass spectrometry and present the first NanoSIMS analyses of H_2O on remelted nanogranites. This cutting-edge analytical tool, useful to quantify volatile concentrations with the potential for submicrometric spatial resolution, has been recently applied to the study of volcanic phenocryst-hosted MI (Hauri et al., 2011) and of nominally anhydrous minerals (Mosenfelder et al., 2011). Our novel approach, resulting from the combination of nanogranite inclusions and NanoSIMS, permits in situ measurements of the H_2O content of any specific granitic melt produced in the partially melted Earth's middle-to-lower continental crust. The presented NanoSIMS data are used to discuss the potential post-entrapment modifications occurring in the studied MI, the H_2O contents of natural granitic

128 melts at the source region, and the mechanisms that may lead to the observed
129 heterogeneities.
130
131 **2. MI entrapment during cooling vs. heating: the conceptual model**
132 Primary MI in peritectic phases of regionally metamorphosed and partially melted crustal
133 rocks represent a novel petrologic tool, their occurrence being described only in a few
134 recent papers (e.g. Bartoli et al., 2013b; Cesare et al., 2009, 2011; Darling, 2013; Ferrero et
135 al., 2012, 2014; Gao et al., 2012, 2013). Conversely, MI in minerals from igneous rocks
136 were first recognized in the 19th century by Sorby (1858), and the studies using or
137 mentioning them have grown to the present level of about 200 per year (see Kesler et al.,
138 2013). Among them, the majority deals with MI in olivine phenocrysts, as they are
139 generally considered to be pristine MI (see Danyushevsky et al., 2002; Frezzotti, 2001;
140 Schiano, 2003; and references therein). Owing to the lack of a thorough theoretical
141 treatment comparing these two different modes of entrapment and their consequences on
142 MI compositions, one might expect the MI formed in migmatitic and granulitic terranes to
143 be involved in, and affected by, the same processes occurring in olivine-hosted MI in
144 magma plumbing systems. Here we show that this is not the case, and discuss some key
145 differences between the two modes of occurrence, from entrapment mechanisms to post-
146 entrapment processes (Fig. 1) before presenting and interpreting the collected data.
147 During ascent and eruption, basaltic magmas are generally close to their liquidus
148 temperature (1100-1300 °C) and follow a nearly adiabatic path. Because olivine is the low-
149 pressure liquidus phase in mantle-derived magmas (Fujii and Kushiro, 1977), olivine
150 phenocrysts form along this crystallization path, trapping droplets of the melt from which
151 they are crystallizing (path b in Fig. 1). Hence olivine-hosted MI may record the

composition of basaltic melts at the liquidus curve (i.e. a parental melt; Fig. 1); however they do not necessarily reflect the melt produced at mantle depths at the onset of peridotite melting (i.e. a primary melt). This is because olivine does not constitute a peritectic phase that forms during partial melting and generation of the mantle magma, but a mineral that crystallizes during the evolution of the magma upon its ascent to the Earth´s surface (Danyushevsky et al., 2000).

On the other hand, the continental crust melts at $T \geq 650$-700 °C, commonly via incongruent reactions of the form, e.g. biotite + sillimanite + plagioclase + quartz = liquid + garnet, with growth of solid phase(s) in the presence of a melt of fixed (peritectic) composition, and with the possibility of MI entrapment (paths a and a' in Fig. 1). In this scenario where the mineral host and the melt form at the same time, the trapped MI record the primary composition of near-solidus anatectic melts (Fig. 1), along a non-adiabatic heating path related to the specific orogenic setting.

The two contrasting mechanisms of primary MI entrapment described above (i.e. entrapment on the liquidus during crystallization of magmas vs. entrapment on, or close to, the solidus during incongruent melting), together with the contrasting P-T histories commonly recorded in the two settings (Fig. 1), also result in different post-entrapment processes affecting the volatile (H_2O) content of the trapped melts.

When mass transport by diffusion is considered, the mass flux vector is composed of four contributions (see equation 5.87 in Brodkey and Hershey, 2003): i) mass diffusion due to concentration gradients, ii) pressure diffusion, iii) mass transport due to external forces, and iv) thermal diffusion (Soret effect). Given the small size (5-15 μm) of MI, contributions iii) and iv) are negligible, so that only the first two mechanisms should be operative. This means that the potentially driving forces for H_2O diffusion from/to MI at

supersolidus conditions are gradients of concentration and/or pressure. For diffusion driven by concentration gradients (i.e. gradients of chemical potentials in thermodynamic terms), Fick's second law indicates that the time (t) needed for a diffusing species to equilibrate is proportional to the square of the diffusion distance (x), but inversely proportional to its diffusivity (D):

$$x \approx \sqrt{Dt} \quad (1)$$

(from Crank, 1975; Zhang, 2010).

During its ascent, a wet basaltic magma may exsolve an aqueous fluid as a natural consequence of near-isothermal decompression and eruption, but the MI trapped in olivine phenocrysts are resistant to degassing due to the isochoric behavior of the melt in the inclusion (path b in Fig. 1). Indeed, the internal pressure of these MI remains virtually unchanged at supersolidus temperatures, and can be several kbar greater than that of the magma hosting the phenocryst (Fig. 1) inhibiting the exsolution of volatiles within MI during magma ascent. In such situations, important gradients of H_2O concentration [contribution i) to diffusion] and pressure [contribution ii) to diffusion] may be continuously established between the melt within inclusions and the external magma, forcing diffusion of hydrogen/molecular H_2O out of MI. Given the coupling of very high hydrogen diffusivities in olivine at T> 1100 °C (D~10^{-9}-10^{-11} m^2/s; Farver, 2010; Hauri, 2000) with the small size of olivine phenocrysts –and hence very short distances between MI and the host boundary (tens to hundreds of μm)–, olivine-hosted MI within magma batches represent the most suitable system for diffusional H_2O re-equilibration, as recently demonstrated by experimental studies (e.g. Chen et al., 2011, 2012; Gaetani et al., 2012; Massare et al., 2002; Portnyagin et al., 2008).

199 Compared with magma plumbing systems, the conditions and evolution of
200 migmatitic and granulitic terranes are very different. When crystalline rocks experience
201 prograde anatexis at temperatures close to their solidus (paths a and a' in Fig. 1), MI-
202 bearing peritectic phases are expected to coexist with discrete fractions of melt scattered as
203 pockets and films in a predominantly solid matrix. Under these conditions the extent of
204 H_2O diffusional re-equilibration between MI and the external matrix would be less than that
205 in mantle magmas due to: i) the lower temperatures resulting in much lower (up to five-
206 seven orders of magnitude) hydrogen diffusivities in silicate minerals ($D \sim 10^{-11}$-10^{-16} m^2/s at
207 700-800 °C; Farver, 2010), ii) the lack of significant pressure gradients between inclusion
208 and external matrix at conditions slightly above the solidus, i.e. the absence of driving force
209 for pressure diffusion (Fig. 1), and iii) the commonly larger grain size of peritectic minerals
210 in high-grade metamorphic rocks and hence the longer diffusion distances between MI and
211 the mineral boundary (a few mm to several cm). Taking into account equation (1), the large
212 differences in physical parameters reported above can account for equilibration times
213 regarding hydrogen between MI and matrix melt much greater (>10 order of magnitudes) in
214 anatectic terranes compared to plumbing magmatic systems. The infiltration of H_2O-rich
215 fluids into the migmatitic front would increase the H_2O contents of matrix melt, likely
216 imposing a concentration gradient towards MI. Because, when a rock is partially melted,
217 melt occludes all the pores even at the lowest degrees of melting (Acosta-Vigil et al., 2006),
218 the mass transfer of aqueous fluid must take place via diffusion through the melt. However,
219 calculations based on diffusivity of H through hydrous but H_2O-undersaturated granitic
220 melts indicate that the new a_{H_2O} will be imposed to the entire melt reservoir over long
221 timeframes –e.g. 30 Ma to 3 Ga in the case of an anatectic front of 100 m to 1 Km in
222 dimension (Acosta-Vigil et al., 2012b). These timeframes represent an additional obstacle

to the H_2O re-equilibration between MI and the matrix melt. Upon cooling, the only major driving force for H diffusion may then be a concentration gradient generated by the deep infiltrations of near-surface H_2O-rich fluids (Yardley et al., 2014) that break down the original assemblage (see reaction 6 in Fig. 1), potentially resulting in H_2O gain to MI.

Additional complexity may arise if crustal melting continues up to temperatures much higher (100-200 °C) than trapping temperature (not shown in Figure 1). In this case the amount of melt in the rock matrix may strongly increase, becoming progressively drier. This situation can potentially produce the diffusive H_2O re-equilibration through the peritectic hosts, i.e. MI may lose a fraction of their initial H_2O content. It is important, however, to note that melt may be rapidly drained from the high-temperature anatectic zones, leaving residual granulites enriched in peritectic minerals (Brown, 2013). High-temperature conditions, therefore, do not implicitly indicate that MI within porphyroblasts experienced diffusive H_2O re-equilibration

3. Samples and methods

The MI studied in this work are hosted in peritectic garnet of Ronda migmatites (Betic Cordillera, S Spain; N 36°36□37.6□, W4°49□15.6□). These rocks have been interpreted as formed during the tectonic emplacement of a mantle slab (i.e. the Ronda peridotites; Obata, 1980) over metasedimentary sequences, producing high-temperature metamorphism and partial melting in the underlying crustal rocks (Acosta-Vigil et al., 2001; Tubía et al., 1997). The studied migmatites are metatexites showing a stromatic structure with thin layers of leucosome surrounded by a fine-grained mesocratic matrix (Fig. 2a). They show a stable mineral assemblage composed of biotite, fibrolitic sillimanite, garnet, graphite,

quartz, plagioclase and K-feldspar (Bartoli et al., 2013c). MI-bearing garnets occur as small (50-200 µm in diameter) crystals both in leucocratic domains (Fig. 2b) and close to the biotite+sillimanite clusters (Fig. 2c) that define the foliation in the rock. Phase equilibria modeling constrains the formation of peritectic garnet at T=660-700 °C and P=4.5-5 kbar (Fig. 3a). Tiny (~ 5 µm) primary inclusions of melt occur in the garnet core (Fig. 2) and mostly appear now as nanogranites containing quartz, muscovite, biotite, plagioclase and rare K-feldspar (Fig. 3b). Partially crystallized inclusions may coexist along with nanogranites in the same MI cluster. To recover complete compositional data, nanogranites have been remelted using a piston cylinder apparatus at conditions (700 °C, 5 kbar) that approach those of trapping (see Bartoli et al., 2013a). Experimental remelting under high-confining pressure prevents MI decrepitation (Bartoli et al., 2013a; Esposito et al., 2012), producing the complete rehomogenization of nanogranites (Fig. 3c). Because MI experimentally remelted at 700 °C do not show clear evidences of overheating (such as irregular walls, cuspate corners and occurrence of peritectic phases produced by incongruent melting of garnet at the MI walls), trapping temperatures lower than 670-680 °C are unreasonable. Quenched glass obtained from remelting experiments at 700 °C displays a peraluminous leucogranitic composition (Bartoli et al., 2013b) in agreement with results from melting experiments of metasedimentary rocks (Clemens, 2006). Some CO_2 is dissolved in the melt, as suggested by the presence of exsolved CO_2 vapor bubbles formed after experiments conducted at temperatures higher than 700 °C (Bartoli et al., 2013a, b).

After a detailed optical and Scanning Electron Microscope (SEM) investigation of the experimental run products to check for MI homogeneity and absence of cracks in host minerals, we identified 26 remelted nanogranites in 8 garnet crystals for determination of H_2O abundance in glasses. Analyses were performed using the Cameca Nano Secondary

Ion Mass Spectrometry 50 (NanoSIMS) installed at Muséum National d'Histoire Naturelle (Paris). Polished experimental capsules with MI exposed on the garnet surface and standard glasses were mounted in In (Aubaud et al. 2007). MI were identified by collecting secondary ion images of Si, K and Fe. For every analysis location, we first performed a pre-sputtering step on a 3x3 μm^2 surface area for 2 minutes with a 400 pA primary Cs^+ beam to remove the gold coating, surface contamination and to reach a steady state sputtering regime. Then a primary beam of 37 pA was used for data acquisition. Data were acquired by rastering a 3x3 μm^2 surface area and collecting only ions from the inner 1x1 μm^2 (beam blanking mode) to reduce surface contamination (Fig. 4a). Each analysis is a stack of 200 cycles, a cycle being 1.024s long. $^{16}OH^-$ (used as a proxy for H_2O), $^{28}Si^-$, $^{39}K^{16}O^-$ and $^{56}Fe^{16}O^-$ were recorded simultaneously in multicollection mode. We checked that $^{16}OH^-$ /$^{28}Si^-$ ratio was stable during MI analyses (see Supplementary material). Secondary ions were collected by electron multipliers with a dead time of 44 ns. Mass resolution was set to 10000. One inclusion was large enough for replicated analyses. For NanoSIMS calibration we used a 5.5 wt% H_2O-bearing leucogranitic glass from Acosta-Vigil et al. (2003), a 4.3 wt% H_2O-bearing leucogranitic glass from Behrens and Jantos (2001) and an anhydrous leucogranitic glass from Morgan and London (2005) (Fig. 4b). Data corrections, using the aforementioned calibration, and error calculations were performed using the R program. Errors combine counting statistic and uncertainty of the calibration curve (Fig. 4b). However, the errors reported in Table 1 are dominated by the uncertainty of the calibration curve, which corresponds to prediction interval at 68%. During the session, the vacuum in the analysis chamber remained between 2.5 and 5 $x10^{-10}$ Torr.

The major-element composition of some MI was obtained before NanoSIMS analysis using a JEOL JXA 8200 Electron Microprobe (EMP) at the Dipartimento di

294 Scienze della Terra, Università di Milano (Italy). Analytical parameters were as follows: 15
295 kV accelerating voltage, 2nA current and a counting time of 10 sec on peak and 2 sec on
296 background. The micrometre scale of the MI required the use of a focused beam with size
297 of ~1 µm. To overcome the alkali loss during EMP measurements, we followed the
298 analytical recommendations of Morgan and London (1996, 2005) and analyses were
299 corrected by using secondary leucogranitic glass standards with H_2O contents as close as
300 possible to the target samples. Details concerning the composition and provenance of the
301 standard glasses are given by Bartoli et al. (2013b) and Ferrero et al. (2012). During
302 analysis, the loss of Na and K was estimated as 26% and 12% relative respectively.
303

304 **4. Results and discussion**

305 *4.1 H_2O contents*

306 The H_2O concentrations of the remelted nanogranites determined by NanoSIMS span a
307 wide range of values from 4.7 to 9.8 wt% (mean value of 6.5±1.4 wt%; Table 1 and Fig. 5).
308 Replicated analyses within a single inclusion show similar H_2O content within error and
309 therefore an homogeneous distribution of H_2O. Comparing NanoSIMS analyses collected
310 from MI within the same host garnet crystal, most MI show relatively uniform H_2O
311 concentrations (standard deviations up to ~13% of the mean concentrations; Fig. 5).
312 However, in two garnet crystals (OB8-7 and OB3-2) the H_2O contents of coexisting re-
313 melted nanogranites may differ significantly (up to 38 and 41% relative, respectively; Fig.
314 5). For instance, a variation of 1-1.5 wt% is observed between two MI separated by only 30
315 µm. No systematic relationships are observed between the melt H_2O content and the
316 microstructural position of MI in the host, i.e. the distance to the core. H_2O estimated by
317 EMP-difference, i.e. differences of EMP totals from 100 %, generally yields slightly higher

318 H_2O contents, up to approximately 15 % relative (Table 1), and only in one inclusion H_2O
319 by difference is ≈25 % relative higher. The NanoSIMS mean values for the MI in different
320 host crystals range from 5.4 to 9.1 wt % (Fig. 5), in agreement with experimental models
321 that predict H_2O contents in granitic melts from approximately 6 to 10 wt% at the P-T
322 conditions inferred for melt formation and entrapment (Fig. 3a), depending if the melt is
323 undersaturated or saturated in an aqueous fluid. Indeed, the liquidus and H_2O-solubility
324 curves for eutectic or minimum compositions in the system Qz-Ab-Or-H_2O (Fig. 3a) are
325 considered to predict adequately the minimum and maximum H_2O contents in granitic
326 melts at the appropriate P-T conditions (Holtz and Johannes, 1994; Holtz et al., 2001).
327 However, natural rocks are more complex than a model composition such as the
328 haplogranite system. For example, for each silicate phase-H_2O (sub)system (e.g.
329 plagioclase-H_2O system) there is a wide field in which the H_2O content of melt is poorly
330 constrained (cf. Fig. 3 in Robertson and Wyllie, 1971). Moreover, Behrens and Jantos
331 (2001) observed that additional components (e.g. Mg, Fe, Ca and Li) play an important role
332 on H_2O solubility in granitic melts. Additional components stabilize Fe-Mg phases, notably
333 biotite and garnet, therefore modifying the liquidus surface at H_2O-undersaturated
334 conditions. This suggests that the H_2O contents predicted by model compositions such as
335 the haplogranitic system have to be considered as approximate values when applied to the
336 case of natural melts.
337 Previous attempts to measure H_2O in remelted nanogranites included in Grt from
338 the same migmatite, using Raman spectroscopy and SIMS, provided similar ranges but
339 lower concentrations of 3.1-7.6 wt% and 2.3-8.1 wt%, respectively (Bartoli et al. 2013a, b).
340 Because the large beam of SIMS sputtered not only glass of the remelted MI but also
341 material from the host crystal, the underestimation of SIMS data with respect to those

342 collected by NanoSIMS is likely due to the assumptions made during mass balance
343 calculations to correct the SIMS measurements (see Bartoli et al., 2013a). Raman
344 spectroscopy is considered a valuable method for H_2O analysis of glassy MI owing to the
345 high-spatial resolution and non-destructive nature of this method (e.g., Thomas, 2000).
346 However, different protocols were proposed in the relevant literature for the acquisition and
347 processing of spectra (e.g., Behrens et al. 2006; Chabiron et al., 2004; Le Losq et al. 2012;
348 Thomas, 2000), and different spectra treatments may significantly affect the resulting
349 estimates (Behrens et al. 2006; Zajacz et al. 2005). A comprehensive understanding of the
350 discrepancy between Raman and NanoSIMS data is beyond the scope of this paper and
351 would require an independent "ad hoc" test of techniques on standard glasses. However, it
352 is important to note that i) the discrepancy is only moderate (approximately 20 % relative
353 on the average value), and ii) the H_2O contents inferred by difference of EMP totals from
354 100 % are in better agreement with the NanoSIMS values.
355
356 *4.2. Reliability of the melt inclusions data*
357 The most evident feature of the dataset presented in Table 1 is the spread of H_2O contents
358 measured in remelted nanogranites. However, before using these H_2O concentrations to
359 make inferences about processes during anatexis and generation of crustal granites we have
360 to assess to what extent the H_2O variations are primary or could be caused by H_2O loss or
361 gain.
362 Our remelting experiments were performed both under dry and H_2O-added
363 conditions with a run duration of 24 h (Bartoli et al., 2013b), and previous Raman
364 spectroscopy measurements yielded similar H_2O contents in MI rehomogenized during dry
365 and wet runs (Bartoli et al., 2013b). Moreover, nanogranite rehomogenization occurred at a

366 temperature (700 °C) similar to, or approaching that, of trapping. These observations refute
367 concerns about the occurrence of H_2O loss during piston cylinder remelting experiments at
368 700 °C, such that our data, obtained from remelting under dry conditions, can be considered
369 reliable.

370 In nature, H_2O loss from MI may occur both above the solidus, where molecular
371 H_2O is dissolved into the melt, and below the solidus, where H_2O is mostly present in the
372 studied MI as liquid H_2O in micro- and nano-bubbles or structurally bound within any
373 remaining glass within MI (see Bartoli et al., 2013b). Mechanisms responsible for the H_2O
374 loss from MI at suprasolidus conditions are the diffusion of hydrogen and molecular H_2O
375 through the host (e.g. Danyushevsky et al., 2002; Frezzotti, 2001; Severs et al., 2007). As
376 noted above, however, diffusion processes would require a driving force, i.e. gradients in
377 molecular H_2O/hydrogen chemical potential or in pressure (see Section 2). To the best of
378 our knowledge, no arguments can be found to support the existence of these processes in
379 the studied rocks. Indeed, Ronda metatexites did not experience $T \geq 750$ °C and the
380 associated high degree of melting with formation of large amounts of high-temperature,
381 H_2O-poor matrix melts and marked MI overpressure. This situation would have favored the
382 H_2O/hydrogen reequilibration between MI and external melt (see Section 2). Severs et al.
383 (2007) observed that H_2O loss may result in the formation of empty bubbles within MI. On
384 the other hand, Danyushevsky et al. (2002) suggested that the loss of H_2O by diffusive re-
385 equilibration of H^+ between the MI and external magma should produce Fe-oxides within
386 MI as a result of H_2O dissociation that increases the oxidation state of Fe. The absence of
387 these textures in the studied MI supports the negligible role played by diffusive H_2O re-
388 equilibration. Gaetani et al. (2012) have shown that molecular H_2O loss at weight-percent
389 levels may force the exsolution of CO_2 into vapor bubbles as a result of large pressure

390 drops within MI. In fact, we have artificially generated CO_2 vapor bubbles within some MI
391 remelted at temperatures (750 and 800 °C) higher than the original temperature of
392 entrapment, where MI decrepitation resulted in H_2O loss, a drop in pressure and
393 vesiculation of CO_2 bubbles (Bartoli et al., 2013a). From all these considerations we
394 conclude that diffusive loss of molecular H_2O and hydrogen did not appreciably affect MI
395 H_2O contents.

396 Concerning the loss of H_2O at subsolidus conditions, the occurrence of cracks at the
397 nanoscale close to MI cannot be ruled out (see Vityk et al. 2000; Ferrero et al. 2011).
398 However, the existence of liquid H_2O-filled micropores and nanopores that have survived
399 for several m.y. in the studied nanogranites (see Fig. 4 in Bartoli et al., 2013b) suggests that
400 the fluid leakage along dislocations in the host mineral had limited influence on the MI
401 H_2O budget. In addition, there is no evidence of retrograde fluid infiltration in the rock
402 matrix and within garnet crystals such as retrograde chlorite replacing biotite and garnet.

403 Despite the range shown by collected data, H_2O contents of MI from the same host
404 crystal are remarkably uniform for the majority of garnets (Fig. 5). Although we cannot rule
405 out that the leakage of fluid along nanocracks might have affected H_2O contents of some
406 MI in a few garnet crystals (e.g. garnet OB8-7, Fig. 5), all the above considerations suggest
407 that, when the entire population from the same host crystal is considered, MI may provide
408 reliable indications of the H_2O content of melt in the specific volume of rock surrounding
409 the growing peritectic host.

410

411 *4.3 Melt compositional heterogeneity at the source region*

412 The occurrence of similar H_2O contents in different MI in the same host (see above) and the
413 lack of chemical zoning in rock-forming minerals (Bartoli et al., 2013c) suggest that the

414 H_2O content of melt fractions were close to equilibrium with the surrounding solid matrix
415 at the time the MI were trapped. This is also supported by observation that the remelting
416 temperature of nanogranite inclusions (~700 °C) conforms to what is predicted by phase
417 equilibria (Fig. 3a). The observed range of mean H_2O contents (5.4 to 9.1 wt %) suggests
418 the presence of heterogeneities of the anatectic melts at the source region. Although
419 disequilibrium in a rapidly heating rock volume cannot be excluded *a priori*, here we
420 propose an explanation for these heterogeneities based on equilibrium behaviour.
421 According to Bartoli et al. (2013b, c), partial melting in the studied migmatites started in
422 the presence of an aqueous fluid phase produced by the subsolidus devolatilization of
423 hydroxylated phases, and melt was trapped in peritectic garnet at 680-700 °C. Under these
424 conditions, and taking into account that the rock is graphitic, a possible cause of
425 heterogeneity may be "mosaic" or domainal equilibrium affecting the activity of H_2O in the
426 fluid attending melting. At given P and T and under fluid-saturated conditions, the amount
427 of H_2O that can be incorporated in a granitic melt is dependent on the composition of the
428 fluid phase coexisting with melt. When the intergranular fluid is in contact with the
429 graphite crystals randomly distributed in the rock matrix, that specific domain is required to
430 contain a graphite-saturated COH fluid, where H_2O activity must be <1 owing to the
431 presence of diluting carbonic species such as CH_4 and/or CO_2 (Connolly and Cesare, 1993).
432 Elsewhere, in the graphite-free domains, the fluid can be pure H_2O. Therefore, just after
433 entering suprasolidus conditions, before melt connectivity is attained, the first coexisting
434 discrete fractions of melt produced in different microdomains (graphite-bearing vs.
435 graphite-free) may contain different amounts of H_2O. When the fluid phase in the rock is
436 essentially produced by H_2O release from phyllosilicates, the X_o (atomic fraction of oxygen
437 relative to oxygen+hydrogen) in the fluid is constrained at 1/3 (Connolly, 1995). Under this

initial condition and at ~5 kbar and ~700 °C, graphite-saturated COH fluids have a maximum a_{H_2O} around 0.83 (calculated considering EoS from Connolly and Cesare, 1993). This scenario can justify the occurrence of coexisting fluid-saturated granitic melts showing H_2O contents from approximately 8 to 10 wt% (Tamic et al., 2001).

It is evident that MI entrapment under fluid-present conditions cannot explain the whole range observed in melt H_2O contents. Assuming that the studied metatexites contain little amounts of aqueous fluid produced by the subsolidus devolatilization of hydrous phases owing to low porosity of crystalline rocks (Sawyer et al, 2011), the system evolves toward a fluid-absent state, for a temperature increase in the range of just a few tens of degrees, i.e. the rock represents a H_2O-deficient (Robertson & Wyllie, 1971), rock-dominated system. MI trapped in the selected garnets may represent a snapshot of this rapid evolution from fluid-present to fluid-absent conditions, occurring over a very small temperature interval (i.e. 10-20 °C) as supported by recent phase equilibria modeling (Bartoli et al., 2013c). In this scenario where some garnets may trap melt formed under fluid-absent conditions, an additional explanation for H_2O heterogeneity can be identified in the control operated on the melt H_2O content by the mineral assemblage of the rock. This process can be explained by considering a model isobaric, isothermal chemography such as an Als-Opx-H_2O section in the K_2O-Na_2O-FeO-MgO-Al_2O_3-SiO_2-H_2O system (Fig. 6, modified after Vielzeuf & Schmidt, 2001). Here, the grey field represents all possible melt compositions in the system at a single P-T condition. Compositional isopleths showing the melt H_2O contents are labeled as c_1 and c_2. Note that these isopleths should be regarded for topological considerations and not for a quantitative application, because the exact location of the liquidus surface in such complex system is still poorly constrained. Figure 6 shows that a bulk composition corresponding to x_1 will be composed by aluminosilicate, garnet,

462 quartz, K-feldspar, plagioclase and a $melt_1$. Likewise, a domain of composition x_2 will
463 contain a $melt_2$ in equilibrium with garnet, quartz, K-feldspar and plagioclase. $Melt_1$ and
464 $melt_2$ show different H_2O contents, c_1 and c_2 respectively (with $c_2 > c_1$), as they pertain to
465 different equilibrium assemblages. It follows that, as metasedimentary rocks often consist
466 of compositionally different domains down to the submillimeter-scale, conditions of
467 "mosaic equilibrium" may be responsible for anatectic melts displaying different H_2O
468 contents. The occurrence of MI-bearing garnet in different microstructural domains of the
469 investigated migmatite (Fig. 2) is consistent with this interpretation even though we do not
470 know the real location of the investigated garnets because they were isolated by crushing
471 the rock. In addition, it is important to note that conditions of "mosaic" equilibrium
472 affecting the activity of H_2O in the fluid phase or the solid assemblages are both compatible
473 with the occurrence of garnet crystals showing similar composition in different portions of
474 the rock, as suggested by phase equilibria modeling (L. Tajcmanova, pers. comm.) and by
475 the chemography of Figure 6.

476 Taking into account all the above considerations, we argue that the range shown by
477 collected data (5.4 to 9.1 wt %) is not inconsistent with primary H_2O concentrations under
478 equilibrium conditions. We attribute this heterogeneity to a local control of different
479 buffering assemblages that pertain to compositionally different microdomains during the
480 rapid evolution of the system from fluid-present to fluid-absent conditions. In such a
481 situation, some peritectic garnets trapped discrete fractions of fluid-saturated melt formed
482 on, or very close to, the wet solidus, whereas other crystals trapped fluid-undersaturated
483 melts produced soon after. Commonly accepted models of crustal anatexis propose that
484 conditions of fluid saturation in melts are rare and limited to the onset of anatexis, and that
485 melting rapidly proceeds by fluid-absent reactions (e.g. Clemens and Vielzeuf, 1987). It

follows that the granitic melt formed under fluid-present conditions should be hardly detectable owing to its imperceptible amounts (Sawyer et al., 2011). The studied MI represent therefore an uncommon and valuable natural occurrence and provide the opportunity to characterize these early formed melts. Finally, by showing that melts may be initially heterogeneous in their source region even for the H_2O content, our study corroborates the conclusions that allochthonous crustal granites can form from individual magma batches with variable compositions that represent, at least in part, heterogeneities inherited from the source (e.g. Deniel et al., 1987; Clemens and Benn, 2010; Pressley and Brown, 1999).

5. Conclusions

Our approach provides an uncommon but well-characterized natural snapshot of the melting process occurring in the Earth's continental crust, and documents for the first time the occurrence of H_2O content heterogeneities of granitic melts at the source region. The most likely explanation for heterogeneities is that compositionally different microdomains in the fertile metasedimentary source result in different equilibrium assemblages (i.e. different buffering assemblages) at the microscale, that play a primary role in constraining the H_2O content of the coexisting discrete fraction of melts during the earliest stages of crustal melting.

NanoSIMS represents the most promising technique to overcome the analytical challenge that the size of nanogranites raises. The same novel approach adopted here on amphibolite-facies migmatites can be successfully extended worldwide to granulitic anatectic terranes, which are thought to be the source region of many upper-crustal granitic magmas. This will lead to the construction of an important and new database on the H_2O

contents of natural granitic melts complementing that proposed by Thomas and Davidson (2012) for variably evolved magmas, that will provide new and additional constraints to the evolution of granitic systems from genesis to emplacement, and to the geochemical, petrological and rheological models on the partially melted continental crust. Because peritectic phases in anatectic rocks seem to be valuable strongboxes where melt compositional heterogeneities at source region can be recorded and preserved, recovering the pristine geochemical signatures hosted in these granite embryos represents a major advance in crustal petrology.

Acknowledgments

The authors thank A. Risplendente for assistance during EMP analyses, and A. Cavallo and L. Peruzzo for help with SEM observations. An anonymous reviewer gave us insightful and constructive comments. We are grateful to L. Tajčmanová for helpful discussions on phase equilibria modeling. Financial support for this project came from the Italian Ministry of Education, University, Research (grant PRIN 2010TT22SC) and from the University of Padua (Progetto di Ateneo CPDA107188/10) to B. Cesare, a research contract from the University of Padua to O. Bartoli, a Ramón y Cajal research contract to A. Acosta-Vigil and grants CGL2007-62992, CTM2005-08071-C03-01, CSD2006-0041, and CNRS to L. Remusat. The National NanoSIMS facility at the MNHN was established by funds from the CNRS , Région Ile de France, Ministère délégué à l'Enseignement supérieur et à la Recherche, and the MNHN.

References

Acosta-Vigil, A., Buick, I., Cesare, B., London, D., Morgan VI, G.B., 2012a. The extent of equilibration between melt and residuum during regional anatexis and its implications for differentiation of the continental crust: a study of partially melted metapelitic enclaves. J. Petrol. 53, 1319–1356.

Acosta-Vigil, A., London, D., Morgan VI, G.B., 2012b. Chemical diffusion of major components in granitic liquids: Implications for the rates of homogenization of crustal melts. Lithos 153, 308–323.

Acosta-Vigil A., Buick I., Hermann J., Cesare B., Rubatto D., London D., Morgan VI G.B., 2010. Mechanisms of crustal anatexis: a geochemical study of partially melted metapelitic enclaves and host dacite, SE Spain. J. Petrol., 51, 785–821.

Acosta-Vigil, A., Cesare, B., London, D., Morgan VI, G.B., 2007. Microstructures and composition of melt inclusions in a crustal anatectic environment, represented by metapelitic enclaves within El Hoyazo dacites, SE Spain. Chem. Geol., 235, 450–465.

Acosta-Vigil, A., London, D., Morgan VI, G.B., 2006. Experiments on the kinetics of partial melting of a leucogranite at 200 MPa H_2O and 690-800 °C: compositional variability of melts during the onset of H_2O-saturated crustal anatexis. Contrib. Mineral. Petrol. 151, 539-557.

Acosta-Vigil A., London, D., Morgan, VI, G.B., Dewers, T.A., 2003. Solubility of excess alumina in hydrous granitic melts in equilibrium with peraluminous minerals at 700–800ºC and 200 MPa, and applications of the aluminium saturation index. Contrib. Mineral. Petrol. 146, 100–119.

Acosta-Vigil, A., Pereira, M.D., Shaw, D.M., London, D., 2001. Contrasting behaviour of boron during crustal anatexis. Lithos, 56, 15–31.

Aubaud, C., Withers, A.C., Hirschmann, M.M., Guan, Y., Leshin, L.A., Mackwell, S.J., Bell, D.R., 2007. Intercalibration of FTIR and SIMS for hydrogen measurements in glasses and nominally anhydrous minerals. Am. Mineral. 92, 811–828.

Bartoli, O., Cesare, B., Poli, S., Acosta-Vigil, A., Esposito, R., Turina, A., Bodnar, R.J., Angel, R.J., Hunter, J., 2013a. Nanogranite inclusions in migmatitic garnet: behavior during piston cylinder re-melting experiments. Geofluids 13, 405–420.

Bartoli, O., Cesare, B., Poli, S., Bodnar, R.J., Acosta-Vigil, A., Frezzotti, M.L., Meli, S., 2013b. Recovering the composition of melt and the fluid regime at the onset of crustal anatexis and S-type granite formation. Geology, 41, 115–118.

Bartoli, O., Tajčmanova B., Cesare B., Acosta-Vigil, A., 2013c. Phase equilibria constraints on melting of stromatic migmatites from Ronda (S. Spain): insights on the formation of peritectic garnet. J. Metam. Geol. 31, 775–789.

Behrens, H., Jantos, N., 2001. The effect of anhydrous composition on H_2O solubility in granitic melts: Am. Mineral. 86, 14–20.

Behrens, H., Roux, J., Neuville D.R., Siemann, M., 2006. Quantification of dissolved H_2O in silicate glasses using confocal microRaman spectroscopy. Chem. Geol. 229, 96–12.

Brodkey, R.S., Hershey, H.C., 2003. Transport phenomena: an unified approach ed. Brodkey publishing, USA.

Brown, M., 2013. Granite: from genesis to emplacement. GSA Bulletin 125, 1079–1113.

Brown, M., Korhonen, F.J., Siddoway, C.S., 2011. Organizing melt flow through the crust. Elements 7, 261–266.

Burnham, C.W., 1967. Hydrothermal fluids at the magmatic stage, in: Barnes, H.L., (Ed.), Geochemistry of Hydrothermal Ore Deposits. New York: Holt, Rinehart and Winston, pp. 34–76.

Burnham, C.W., 1975. Water and magmas: a mixing model. Geochim. Cosmochim. Acta 39, 1077–1084.

Burnham, C.W., Ohmoto, H., 1980. Late-stage processes of felsic magmatism, in: Ishihara, S., Takenouchi, S., (Eds.), Granite magmatism and related mineralization. Mining Geology Special Issue 8, pp. 1–11.

Campbell, I.H., Taylor, S.R., 1983. No H_2O, no granites. No oceans, no continents. Geophys. Res. Lett. 10, 1061–1064.

Candela, P.A., 1997. A review of shallow, ore-related granites: textures, volatiles and ore metals. J. Petrol. 38, 1619–1633.

590 Carrington, D.P., Harley, S.L., 1995. Partial melting and phase relations in high-grade
591 metapelites: an experimental petrogenetic grid in the KFMASH system. Contrib.
592 Mineral. Petrol. 120, 270-291.
593 Cesare B, Acosta-Vigil A, Ferrero S, Bartoli O 2011. Melt inclusions in migmatites and
594 granulites. In: Journal of the Virtual Explorer (eds Forster MA & Fitz Gerald JD),
595 Electronic Edition, ISSN 1441-8142, 38, paper 2.
596 Cesare B, Ferrero S, Salvioli-Mariani E, Pedron D, Cavallo A 2009. Nanogranite and
597 glassy inclusions: the anatectic melt in migmatites and granulites. Geology, 37, 627–
598 630.
599 Cesare, B., Marchesi, C., Hermann, J. & Gomez-Pugnaire, M.T., 2003. Primary melt
600 inclusions in andalusite from anatectic graphitic metapelites: implications for the
601 position of the Al_2SiO_5 triple point. Geology, 31, 573–576.
602 Cesare, B., Salvioli–Mariani, E., Venturelli, G., 1997. Crustal anatexis and melt extraction
603 during deformation in the restitic xenoliths at El Joyazo (SE Spain). Mineral. Mag. 61,
604 15–27.
605 Chabiron, A., Pironon, J., Massare, D., 2004. Characterization of H_2O in synthetic rhyolitic
606 glasses and natural melt inclusions by Raman spectroscopy. Contrib. Mineral. Petrol.
607 146, 485–492.
608 Chen Y., Provost A., Schiano P., Schiano, P., Cluzel, N., 2011. The rate of H_2O loss from
609 olivine-hosted melt inclusions. Contrib. Mineral. Petrol. 162, 625–636.
610 Chen Y., Provost A., Schiano P., Schiano, P., Cluzel, N., 2013. Magma ascent rate and
611 initial H2O concentration inferred from diffusive H2O loss from olivine-hosted melt
612 inclusions. Contrib. Mineral. Petrol. 165, 525–541.
613 Clemens, J.D., 1984. H_2O content of silicic to intermediate magmas. Lithos 17, 273–287.
614 Clemens, J.D., 2006. Melting of the continental crust: fluid regimes, melting reactions and
615 source-rock fertility, in: Brown, M., Rushmer, T. (Eds.), Evolution and Differentiation
616 of the Continental Crust, Cambridge University Press, Cambridge , pp. 297–331.
617 Clemens, J.D., Benn, K., 2010. Anatomy, emplacement and evolution of a shallow-level,
618 post-tectonic laccolith: the Mt Disappointment pluton, SE Australia. J. Geol. Soc.
619 London 167, 915–41.
620 Clemens, J.D., Droop, G.T.R., 1998. Fluids, *P–T* paths and the fates of anatectic melts in
621 the Earth's crust. Lithos 44, 21–36.
622 Clemens, J.D., Holloway, J.R., White, A.J.R., 1986. Origin of an A-type granite:
623 Experimental constraints. Am. Mineral. 71, 317–324.
624 Clemens, J.D., Stevens, G., 2012. What controls chemical variation in granitic magmas?
625 Lithos 134–135, 317–329.
626 Clemens, J.D., Vielzeuf, D., 1987. Constraints on melting and magma production in the
627 crust. Earth Planet. Sci. Lett. 86, 287–306.
628 Clemens, J.D., Wall, V.J., 1981. Origin and crystallization of some peraluminous (S-type)
629 grantic magmas. Can. Mineral. 19, 111–131.
630 Clemens, J.D., Watkins, J.M., 2001. The fluid regime of high-temperature metamorphism
631 during granitoid magma genesis. Contrib. Mineral. Petrol. 140, 600–606.
632 Connolly, J.A.D., 1995. Phase diagrams for graphitic rocks. Contrib. Mineral. Petrol. 119,
633 94–116.
634 Connolly, J.A.D., Cesare, B., 1993. C-O-H-S fluid composition and oxygen fugacity in
635 graphitic metapelites. . J. Metam. Geol. 11, 379–388.
636 Crank, J., 1975. The mathematics of diffusion ed. Clarendon Press, Oxford.

637 Dall'Agnol, L., Scaillet, B., Pichavant, M., 1999. An experimental study of a lower
638 Proterozoic A-type granite from the eastern Amazonian Craton, Brazil. J. Petrol. 40,
639 1673–1698.
640 Danyushevsky, L.V., Della Pasqua, F.N., Sokolov, S. 2000. Reequilibration of melt
641 inclusions trapped by magnesian olivine phenocrysts from subduction-related magmas:
642 petrological implications. Contrib. Mineral. Petrol. 138, 68–83.
643 Danyushevsky, L.V., McNeill, A.W., Sobolev, A.V., 2002. Experimental and petrological
644 studies of melt inclusions in phenocrysts from mantle-derived magmas: an overview of
645 techniques, advantages and complications. Chem. Geol. 183, 5–24.
646 Darling, R.S., 2013. Zircon-bearing, crystallized melt inclusions in peritectic garnet from
647 the western Adirondack Mounatins, New York State, USA. Geofluids 13, 453–459.
648 Deniel, C., Vidal, P., Fernandez, A., Lefort, P., Pecaut, J.J., 1987. Isotopic study of the
649 Manaslu granite (Himalaya, Nepal): inferences of the age and source of Himalayan
650 leucogranites. Contrib. Mineral. Petrol. 96, 78–92.
651 Di Martino, C., Forni, F., Frezzotti, M.L., Palmeri, R., Webster, J.D., Ayuso, R.A., Lucchi,
652 F., Tranne, C.A., 2011. Formation of cordierite-bearing lavas during anatexis in the
653 lower crust beneath Lipari Island (Aeolian arc, Italy). Contrib. Mineral. Petrol. 161,
654 1011–1030.
655 Esposito, R., Klebesz, R., Bartoli, O., Klyukin, Y.I., Moncada, D., Doherty, A.L., Bodnar,
656 R.J., 2013. Application of the Linkam TS1400XY heating stage to melt inclusion
657 studies. Cent. Eur. J. Geosci. 4 208–218.
658 Evensen, J.M., London, D., 2005. Experimental partitioning of Be, Cs, and other trace
659 elements between cordierite and felsic melt, and the chemical signature of S-type
660 granite. Contrib. Mineral. Petrol. 144739–757.
661 Farver, J.R., 2010. Oxygen and hydrogen diffusion in minerals. Rev. Mineral. Geochem.
662 72, 447–508.
663 Ferrero, S., Bartoli, O., Cesare, B., Salvioli-Mariani, E., Acosta- Vigil, A., Cavallo, A.,
664 Groppo, C., Battiston, S., 2012. Microstructures of melt inclusions in anatectic
665 metasedimentary rocks. J. Metam. Geol. 30, 303–322.
666 Ferrero, S., Bodnar, R.J., Cesare, B. & Viti, C., 2011. Reequilibration of primary fluid
667 inclusions in peritectic garnet from metapelitic enclaves, El Hoyazo, Spain. Lithos 124,
668 117–131.
669 Ferrero, S., Braga, R., Berkesi, M., Cesare, B., Ouazaa, L., 2014. Production of
670 metaluminous melt during fluid-present anatexis: an example from the Maghrebian
671 basement, La Galite Archipelago, central Mediterranean. J. Metam. Geol. 32, 209–225.
672 Frezzotti, M.L. 2001. Silicate melt inclusions in magmatic rocks: applications to petrology.
673 Lithos 55, 273–299.
674 Frezzotti, M.L., Peccerillo, A., Zanon, V., Nikogosian, I. 2004. Silica-rich melts in quartz
675 xenoliths from Vulcano Island and their bearing on processes of crustal anatexis and
676 crust-magma interaction beneath the Aeolian Arc, southern Italy. J Petrol 45, 3–26.
677 Fujii, T., Kushiro, I., 1977. Melting relations and viscosity of an abyssal tholeiite, Year
678 Book Carnegie Inst., Washington, 76, 461–465.
679 Gaetani, G.A., O'Leary J.A., Shimizu N., Bucholz, C.E., Newville, M., 2012. Rapid
680 reequilibration of H_2O and oxygen fugacity in olivine-hosted melt inclusions. Geology
681 40, 915–918.

682 Gao, X.Y., Zheng, Y.F., Chen, Y.X., 2012. Dehydration melting of ultrahigh-pressure
683 eclogite in the Dabie orogen: evidence from multiphase solid inclusions in garnet. J.
684 Metam. Geol 30, 193–212.
685 Gao, X.-Y., Zheng, Y.-F., Chen, Y.-X., Hu, Z., 2013. Trace element composition of
686 continentally subducted slab-derived melt: insight from multiphase solid inclusions in
687 ultrahigh-pressure eclogite in the Dabie orogen. J. Metam. Geol 31, 453–468.
688 Giordano, D., Nichols, A.R.L., Dingwell, D.B., 2005. Glass transition temperatures of
689 natural hydrous melts: a relationship with shear viscosity and implications for the
690 welding process. J. Volc. Geoth. Res. 142, 105–118.
691 Goranson, R.W., 1931. The solubility of H_2O in granitic magmas. Am. J. Sci. 22, 481–502.
692 Graybill, F.A., 1976. Theory and Application of the Linear Model, Duxbury, United States.
693 Hauri, E.H., Weinreich, T., Saal, A.E., Rutherford, M.C., Van Orman, J.A., 2011. High
694 Pre-Eruptive H_2O Contents Preserved in Lunar Melt Inclusions. Science 333, 213–215.
695 Hermann, J., 2003. Experimental evidences for diamond-facies metamorphism in the
696 Doira-Maira massif. Lithos 70, 163–182.
697 Holtz, F., Johannes W. 1991. Genesis of peraluminous granites. I. Experimental
698 investigation of melt composition at 3 and 5 kbar and reduced H_2O activity., J Petrol 32,
699 935–958
700 Holtz, F., Johannes, W., 1994. Maximum and minimum H_2O contents of granitic melts:
701 implications for chemical and physical properties of ascending magmas. Lithos 32, 149–
702 159.
703 Holtz, F., Johannes, W., Tamic, N., Behrens, H., 2001. Maximum and minimum H_2O
704 contents of granitic melts generated in the crust: A reevaluation and implications. Lithos
705 56, 1–14.
706 Icenhower, J., London, D., 1995. An experimental study of element partitioning among
707 biotite, muscovite and coexisting peraluminous silicic melt at 200 MPa (H_2O). Am.
708 Mineral. 80, 1229–1251.
709 Johannes, W., Holtz, F., 1996. Petrogenesis and experimental petrology of granitic rocks,
710 Springer, Berlin.
711 Keppler, H. 1989. The influence of the fluid phase composition on the solidus temperatures
712 in the haplogranite system $NaAlSi_3O_8$-$KAlSi_3O_8$- SiO_2-H_2O-CO_2. Contrib. Mineral.
713 Petrol. 102,32l–327.
714 Kesler, S.E., Bodnar, R.J., Mernagh, T.P., 2013. Role of fluid and melt inclusion studies in
715 geologic research. Geofluids
716 Kushiro, I., 1978. Viscosity and structural changes of albite ($NaAlSi_3O_8$) melt at high
717 pressures. Earth Planet. Sci. Lett. 41, 87–90.
718 Le Breton, N., Thompson, A.B., 1988. Fluid-absent (dehydration) melting of biotite in
719 metapelites in the early stages of crustal anatexis. Contrib. Mineral. Petrol. 99, 226–237.
720 Le Losq, C., Neuville, D.R., Moretti, R., Roux, J., 2012. Determination of H_2O content in
721 silicate glasses using Raman spectroscopy: implications for teh study of explosive
722 volcanism. Am. Mineral. 97, 779–790.
723 Lesne, P., Scaillet, B., Pichavant, M., Iacono-Marziano, G., Beny, J-M., 2011. The H_2O
724 solubility of alkali basaltic melts: an experimental study. Contrib. Mineral. Petrol. 162,
725 133–151.
726 Lloyd, A. S., Plank, T., Ruprecht, P., Hauri E.H., Rose, W., 2013. Volatile loss from melt
727 inclusions in pyroclasts of differing sizes. Contrib. Mineral. Petrol. 165, 129–153.

728 Maaløe, S., Wyllie, P.J., 1975. H_2O content of a granite magma deduced from the sequence
729 of crystallization determined experimentally with H_2O-undersaturated conditions.
730 Contrib. Mineral. Petrol. 52, 175–191.
731 Massare, D, Metrichm N, Clocchiatti, R 2002. High-temperature experiments on silicate
732 melt inclusions in olivine at 1 atm: inference on temperatures of homogenization and
733 H_2O concentrations. Chem. Geol. 183, 87–98.
734 Montel, J.-M., Vielzeuf, D., 1997. Partial melting of metagreywackes, Part II.
735 Compositions of minerals and melts. Contrib. Mineral. Petrol. 128, 176–196.
736 Morgan, G.B., London, D., 1996. Optimizing the electron microprobe analysis of hydrous
737 alkali aluminosilicate glasses. Am. Mineral. 81, 1176–1185.
738 Morgan, G.B., London, D., 2005. Effect of current density on the electron microprobe
739 analysis of alkali aluminosilicate glasses. Am. Mineral. 90, 1131–1138.
740 Mosenfelder, J.L., Le Voyer, M., Rossman, G.R., Guan, Y., Bell, D.R., Asimow, P.D.,
741 Eiler, J.M., 2011. Analysis of hydrogen in olivine by SIMS: Evaluation of standards and
742 protocol. Am. Mineral. 96, 1725–1741.
743 Obata, M., 1980. The Ronda peridotite: garnet-, spinel-, and plagioclase-lherzolite facies
744 and the P-T trajectories of a high temperature mantle intrusion. J. Petrol. 21, 533–572.
745 Patiño Douce, A.E., Beard, J.S., 1995. Dehydration-melting of biotite gneiss and quartz
746 amphibolite from 3 to 15 kbar. J. Petrol. 36, 707–738.
747 Patiño Douce, A.E., Johnston, A.D., 1991. Phase equilibria and melt productivity in the
748 pelitic system: implications for the origin of peraluminous granitoids and aluminous
749 granulites. Contrib. Mineral. Petrol. 107, 202–218.
750 Patiño Douce, A.E., Harris, N., 1998. Experimental constraints on Himalayan anatexis. J.
751 Petrol. 39, 689–710.
752 Portnyagin, M., Almeev, R., Matveev, S., Holtz, F., 2008. Experimental evidence for rapid
753 H2O exchange between melt inclusions in olivine and host magma. Earth Planet. Sci.
754 Lett. 272, 541–552.
755 Robertson, J.K., Wyllie, P.J., 1971. Rock-H_2O systems, with special reference to the H_2O-
756 deficient region. Am. J. Sc. 271, 252–277.
757 Sawyer, E.W., 2010. Migmatites formed by H_2O-fluxed partial melting of a
758 leucogranodiorite protolith: microstructures in the residual rocks and source of the fluid.
759 Lithos 116, 273–286.
760 Sawyer, E.W., Cesare, B., Brown, M., 2011. When the continental crust melts. Elements 7,
761 229–234.
762 Scaillet, B., Pichavant, M., Roux, J., 1995. Experimental crystallization of leucogranite
763 magmas. J. Petrol. 36, 664–706.
764 Scaillet, B., Holtz, F., Pichavant, M., Schmidt, M., 1996. Viscosity of Himalayan
765 leucogranites: implications for mechanisms of granitic magma ascent. J. Geoph. Res.
766 101, 27691–27699.
767 Schiano, P., 2003. Primitive mantle magmas recorded as silicate melt inclusions in igneous
768 minerals. Earth Sc. Rev. 63, 121–144.
769 Severs, M.J., Azbej, T., Thomas, J.B., Mandeville, J.B., Bodnar, R.J. 2007. Experimental
770 determination of H_2O loss from melt inclusions during laboratory heating: evidence
771 from Raman spectroscopy. Chem. Geol. 237, 358–71.
772 Shaw, H.R., 1963. Obsidian-H_2O viscosities at 1000 and 2000 bars in the temperature
773 range 700 to 900 °C. J. Geoph. Res. 68, 6337–6343.

774 Sorby, H.C., 1858. On the microscopical structure of crystals, indicating origin of minerals
775 and rocks. Quart. J. Geol. Soc. London 14, 453–500.
776 Spear, F.S., Cheney, J.T., 1989. A petrogenetic grid for pelitic schists in the system SiO_2-
777 Al_2O_3-FeO-MgO-K_2O-H_2O. Contrib. Mineral. Petrol. 101, 149–164.
778 Spicer, E.M., Stevens, G., Buick, I.S., 2004. The low-pressure partial-melting behaviour of
779 natural boron-bearing metapelites from the Mt. Stafford area, central Australia. Contrib.
780 Mineral. Petrol. 148, 160-179.
781 Stevens, G., Clemens, J.D., Droop, G.T.R., 1997. Melt production during granulite-facies
782 anatexis: Experimental data from "primitive" metasedimentary protoliths. Contrib.
783 Mineral. Petrol. 128, 352–370.
784 Stevens, G., Villaros, A., and Moyen, J.F., 2007. Selective peritectic garnet entrainmentas
785 the origin of geochemical diversity in S-type granites. Geology 35, 9–12.
786 Tamic, N., Behrens, H., Holtz, F., 2001. The solubility of H_2O and CO_2 in rhyolitic melts in
787 equilibrium with a mixed CO_2-H_2O fl uid phase: Chemical Geology, v. 174, p. 333–347,
788 Thomas, R, 2000. Determination of H2O contents of granite melt inclusions by confocal
789 laser Raman microprobe spectroscopy. Am. Mineral. 85, 868–72.
790 Thomas, R., Davidson, P., 2012. H2O in granite and pegmatite-forming melts. Ore Geol.
791 Rev. 46, 32–46.
792 Tubía, J.M., Cuevas, J., Gil-Ibarguchi, J.I., 1997. Sequential development of the
793 metamorphic aureole beneath the Ronda peridotites and its bearing on the tectonic
794 evolution of the Betic Cordillera. Tectonophysics 279, 227–252.
795 Tuttle, O.F., Bowen, N.L., 1958. Origin of granite in the light of experimental studies in the
796 system $NaAlSi_3O_8$–$KAlSi_3O_8$–SiO_2–H_2O. The Geological Society of America, Memoir,
797 74.
798 Vielzeuf, D., Holloway, J.R., 1988. Experimental determination of the fluid-absent melting
799 relations in the pelitic system. Contrib. Mineral. Petrol. 98, 257–276.
800 Vielzeuf, D., Schmidt, M.W., 2001. Melting relations in hydrous systems revisited:
801 application to metapelites, metagreywackes and metabasalts. Contrib. Mineral. Petrol.
802 141, 251–267.
803 Vielzeuf, D., Clemens, J.C., Pin, C., and Moinet, E., 1990. Granites, granulites and crustal
804 differentiation, in: Vielzeuf, D., and Vidal, P., (Eds.), Granulites and crustal
805 differentiation. Kluwer Academic Publishers, Dordrecht, pp. 59–85.
806 Vityk, M.O., Bodnar, R.J., Doukhan, J.C. 2000. Synthetic fluid inclusions: XV. TEM
807 investigation of plastic flow associated with re-equilibration of synthetic fluid inclusions
808 in natural quartz. Contrib. Mineral. Petrol. 139, 285–97.
809 Ward, R., Stevens, G., Kisters, A., 2008. Fluid and deformation induced partial melting and
810 melt volumes in lowtemperature granulite-facies metasediments, Damara Belt, Namibia.
811 Lithos, 105, 253–271.
812 Webster, J.D., Rebbert, C.R., 2001. The geochemical signature of fluid-saturated magma
813 determined from silicate melt inclusions in Ascension Island granite xenoliths. Geochim.
814 Cosmochim. Acta 65, 123–136.
815 Webster, J.D., Thomas, R., 2006. Silicate melt inclusions in felsic plutons: a synthesis and
816 review, in: Webster, J.D., (Eds.), Melt inclusions in plutonic rocks. Mineralogical
817 Association of Canada Short Course 36, p. 165–188.
818 White, R.W., Powell, R., 2010. Retrograde melt-residue interaction and the formation of
819 near-anhydrous leucosomes in migmatites. J. Metam. Geol. 28, 579–597.

820 Whitney, D.L., Evans, B.W., 2010. Abbreviations for names of rock-forming minerals.
821 Am. Mineral. 95, 185–187.
822 Yardley, B.W.D., Rhede, D., Heinrich, W., 2014. Rates of retrograde metamorphism and
823 their implications for the rheology of the crust: an experimental study. J. Petrol. 55, 623–
824 641.
825 Zajacz, Z., Halter, W., Malfait, W.J., Bachmann, O., Bodnar, R.J., Hirschmann, M.M.,
826 Mandeville, C.W., Morizet, T., Müntener, O., Ulmer, P., Webster, J.D., 2005. A
827 composition-independent quantitative determination of the H_2O content in silicate
828 glasses and silicate melt inclusions by confocal Raman spectroscopy. Contrib. Mineral.
829 Petrol. 150, 631–642.
830 Zhang, Y., 2010. Diffusion in minerals and melts: theoretical background. Rev. Mineral.
831 Geochem. 72, 5–59.
832

Figure captions

Fig. 1. Two contrasting scenarios of MI formation and post-entrapment processes (see text for details). *Path a* refers to MI trapped by growing peritectic garnet (red dot) close to the wet solidus of a metapelitic crustal section. As demonstrated by Bartoli et al. (2013c), small amounts of peritectic garnet may be formed in metasediemntary rocks at T≤700 °C and at medium-to-low P by continuous melting reactions involving biotite and/or muscovite. During natural cooling, the trapped granitic melt crystallizes forming a cryptocrystalline aggregate named nanogranite. Although crystalline basements may be characterized by very complex polymetamorphic evolutions, a general clockwise P-T path characterized by isobaric heating is assumed here as typical of continental collision settings. *Path a'* as path a, but here partial melting and formation of peritectic garnet begin under fluid-absent conditions, and MI are totally crystallized to nanogranites after crossing their H_2O-undersaturated solidi. *Path b* refers to olivine phenocryst (blue dot) that crystallizing on basaltic liquidus traps a H_2O-saturated melt. Upon rapid cooling through the glass transition temperature, MI are generally quenched to homogeneous glasses. This example only considers a subduction-related (i.e. H_2O-rich) basaltic magma and a closed-system degassing path for simplicity. [1] from Vielzeuf and Schmidt (2001); [2] from Bartoli et al. (2013c); [3] from Patiño Douce and Johnston, (1991); [4]: wet granite solidus (from Hermann et al., 2003); [5]: H_2O-undersaturated haplogranite solidi for given X_{H_2O} in melt (from Johannes and Holtz, 1996); [6] from Spear and Cheney (1989). GT: range of possible glass transition temperatures for basaltic melts (from Giordano et al., 2005). Dashed grey lines refer to schematic isochores followed by MI after entrapment. Dashed black lines refer to H_2O solubility in basaltic melts (from Lesne et al., 2011). Dotted black lines represent the liquidus curves for the haplogranite eutectic or minimum melt composition at specified H_2O contents interpreted to predict the minimum H_2O content of granitic melts (from Holtz et al., 2001). Mineral abbreviations after Whitney and Evans (2010).

Fig. 2. a) Field aspect of the investigated stromatic metatexite at Ronda. b) Photomicrograph of euhedral garnet surrounded by quartz and feldspars. Red arrow: MI cluster. c) Photomicrograph of MI-bearing garnet associated with biotite and fibrolitic sillimanite. Red arrow: MI cluster.

Fig. 3. a) P-T section for stromatic migmatite in the MnO-Na_2O-CaO-K_2O-FeO-MgO-Al_2O_3-SiO_2-H_2-O_2-C system (calculated from Bartoli et al., 2013c). Solid yellow ellipse: inferred P-T conditions for peritectic garnet formation and melt entrapment. Dashed yellow ellipse: shift of the estimated P-T conditions after addition and involvement of the TiO_2 component in the system. (see details in Bartoli et al., 2013c). Grey area: Grt-Bt-Sil-Pl-Kfs-Qz-Gr-COH-Liq stability field corresponding to the observed stable mineral assemblage. Liq-in curve: fluid-saturated solidus. Dotted and dashed blue lines: liquidus curves of the system Qz-Ab-Or for minimum and eutectic compositions and specified H_2O contents (expressed in wt %). Dotted lines are from Holtz and Johannes (1994). Dashed lines are from Holtz et al. (2001). The discrepancy between the two sets of liquidus curves results from the different H_2O solubility data used in the calculations (see Holtz et al., 2001). Dotted black lines: H_2O solubility isopleths for minimum and eutectic compositions in the

system Qz-Ab-Or (from Johannes and Holtz, 1996). b) SEM BSE image of nanogranite inclusions in garnet (Grt). Melt inclusions have a typical negative crystal shape and display a diffuse micro- to nanoporosity (white arrows), which contains liquid H_2O, as evidenced by micro-Raman mapping (Bartoli et al. 2013b); c) SEM BSE image of a MI completely re-homogenized at 700 °C and 5 kbar by piston cylinder. MI consists of an homogeneous glass and still preserves the negative crystal shape, suggesting that no host garnet (Grt) dissolved into the melt during heating experiments, and therefore that the trapping temperature was not significantly exceeded.

Fig. 4. a) NanoSIMS correction curve used for this session. D, LGB1 and DL are leucogranitic glass standards with 0, 4.3 and 5.5 wt% H_2O respectively (see text for details). Replicates on each standard are reported. We assumed that the relationship between OH/Si and H_2O content remains linear beyond 5.5 wt% H_2O. For each measurement, errors arising from counting statistics are smaller than the symbol. The spread represents the reproducibility in the course of the session. The linear regression and the prediction interval (at 68%) were determined thanks to the R program, using the Graybill method (Graybill, 1976). OH/Si stands for the $^{16}OH^-/^{28}Si^-$ determined by NanoSIMS. Detection limit can be estimated at 0.33 wt% for H_2O content in our analytical conditions. b) BSE image of melt inclusion showing the typical 3x3 μm^2 pit (white arrow) produced during NanoSIMS analysis. White square represents the inner 1x1 μm^2 area from which ions were collected (see text for details).

Fig. 5. H_2O concentration of re-homogenized nanogranite inclusions from eight garnet crystals determined by NanoSIMS. Black dots are averages within each garnet. White dot reflects average of all melt inclusions. Horizontal bars are one standard deviation on average values. In one case, standard deviation is smaller than the symbol. The number of analyses is indicated next to horizontal bars.

Fig. 6. Isobaric, isothermal section for metapelites and metagreywackes in the K_2O- Na_2O-FeO-MgO- Al_2O_3-SiO_2-H_2 system at 950 °C and 10 kbar (redrawn after Vielzeuf and Schmidt, 2001). Grey area: compositional field of melt. C_1, c_2: melt H_2O content isopleths. X_1, x_2:compositionally different domains. See text for details.

914 **Table 1.**

915 H_2O concentrations measured in re-homogenized melt inclusions by NanoSIMS

Sample	H2O content (wt %)	1σ error	$^{16}O^{1}H^{-}/^{28}Si^{-}$
OB8-1_1	5.6	0.3	1.66E-01
OB8-1_2	5.6	0.3	1.66E-01
5.6 (0.01)[a]			
OB8-3_1	4.7	0.3	1.40E-01
OB8-3_2[b]	5.2	0.3	1.56E-01
OB8-3_3[b]	5.5	0.3	1.62E-01
OB8-3_6	5.3	0.3	1.57E-01
OB8-3_7	6.1	0.3	1.80E-01
5.4 (0.57)[a]			
OB8-4_1	5.2	0.3	1.55E-01
OB8-4_2	5.0	0.3	1.50E-01
OB8-4_3	6.2	0.3	1.84E-01
OB8-4_4	6.4	0.3	1.89E-01
OB8-4_5	6.0	0.3	1.77E-01
OB8-4_8	5.8	0.3	1.72E-01
5.5(0.55)[a]			
OB8-5_1	6.9	0.3	2.05E-01
OB8-5_2	6.0	0.3	1.77E-01
OB8-5_3	5.4	0.3	1.61E-01
6.1 (0.79)[a]			
OB8-7_2	9.2	0.3	2.69E-01
OB8-7_3	6.4	0.3	1.89E-01
OB8-7_4	5.4	0.3	1.62E-01
OB8-7_5	6.4	0.3	1.90E-01
6.8 (1.61)[a]			
OB3-1_3	9.1 (8.9)[d]	0.3	2.68E-01
OB3-2_4	8.4 (8.2)[d]	0.3	2.48E-01
OB3-2_5	6.8 (8.1)[d]	0.3	2.00E-01
OB3-2_6	5.2 (7.1)[d]	0.3	1.56E-01
6.8 (1.60)[a]			
OB3-3_7	8.4 (9.0)[d]	0.3	2.46E-01
OB3-3_8	9.8 (11.1)[d]	0.4	2.86E-01
OB3-3_9	7.8 (8.6)[d]	0.3	2.30E-01

	8.7 (1.01)[a]
	6.5 (1.42)[c]

[a] Average value and 1σ standard deviation (in parentheses) regarding NanoSIMS measurements from the same host crystal

[b] Repeated analyses on the same inclusion

[c] Average value and 1σ standard deviation (in parentheses) regarding all the NanoSIMS measurements

[d] H_2O contents estimated by difference of EMP totals from 100 % are reported between parentheses and are close to the NanoSIMS values obtained for the same MI

916

Highlights:

- First time in literature of NanoSIMS applied on nanogranite inclusions;

- H_2O content of embryos of the upper-crustal anatectic granites;

- Mean H_2O values for the selected host crystals between 5.4 and 9.1 wt%;

- H_2O content heterogeneities of granitic melts at the source region

Figure

Click here to download high resolution image

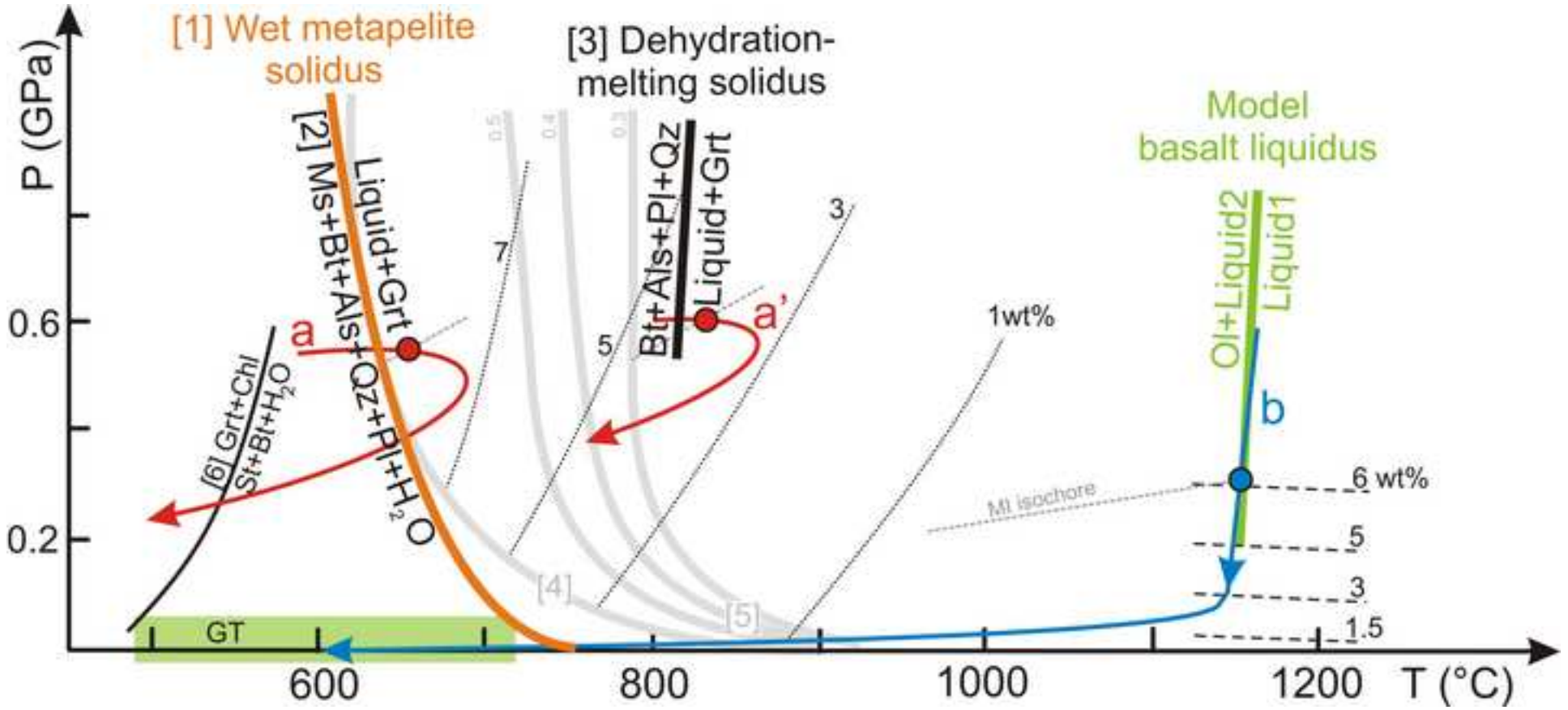

Figure

Click here to download high resolution image

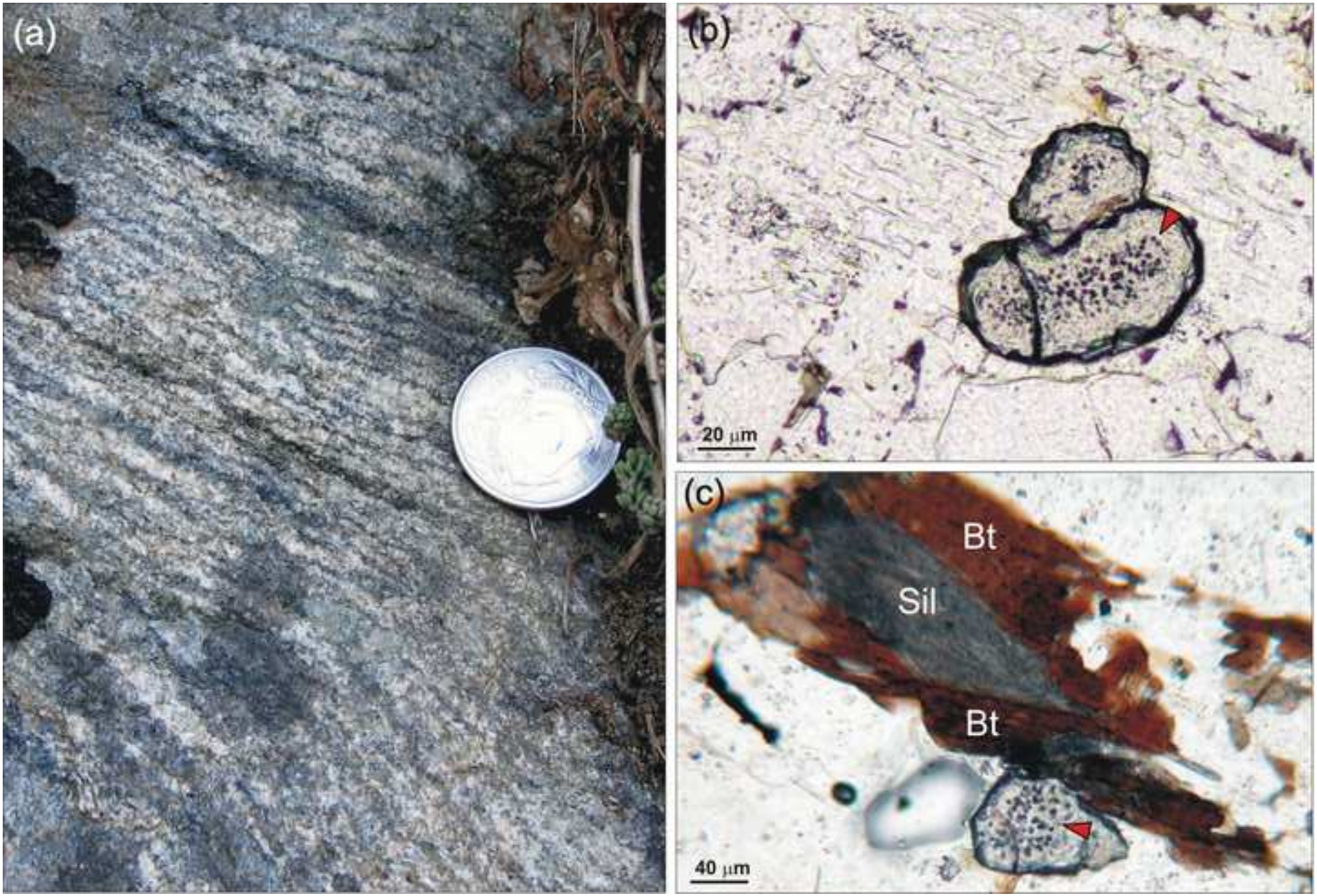

Figure
Click here to download high resolution image

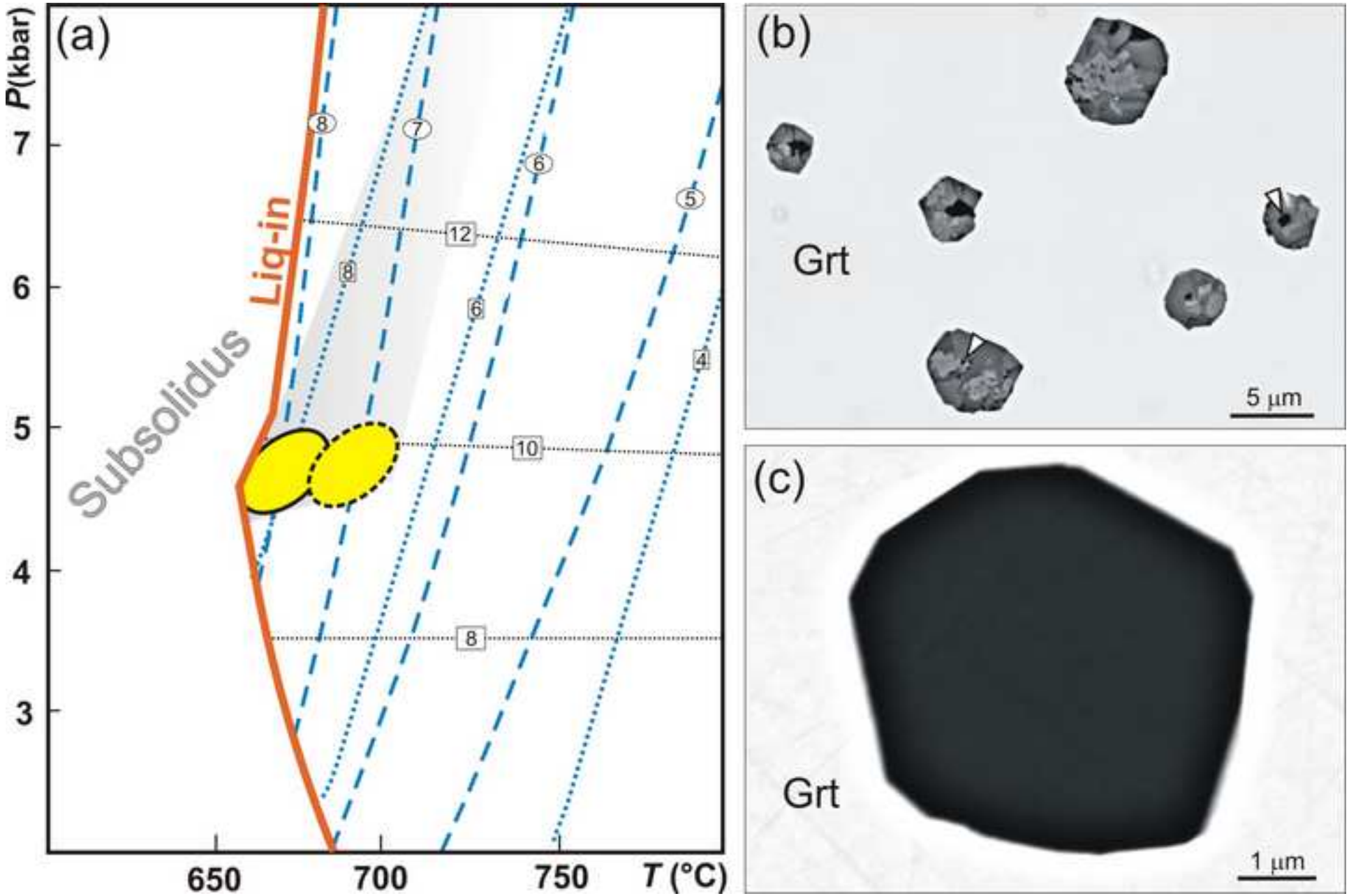

Figure

Click here to download high resolution image

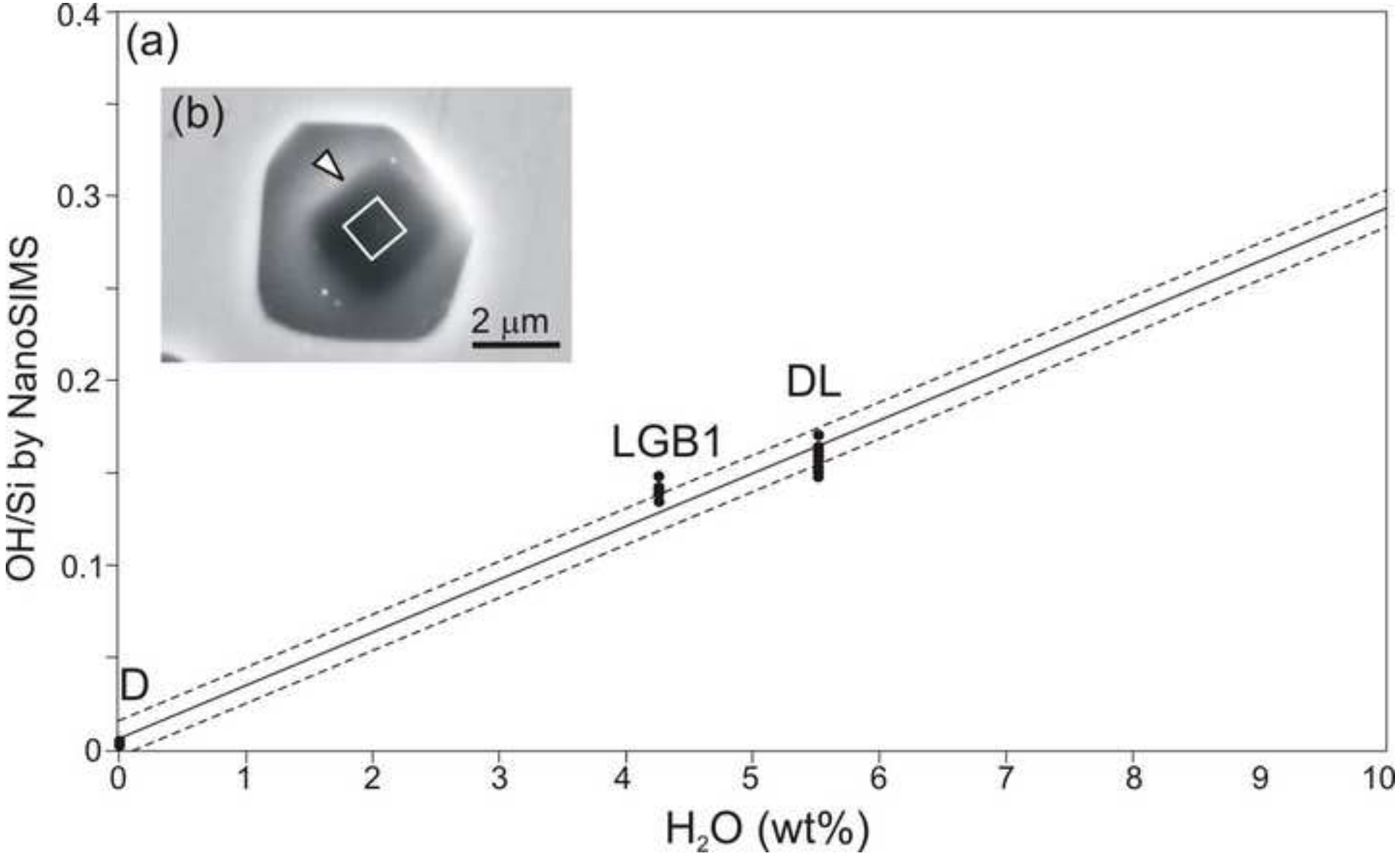

Figure
Click here to download high resolution image

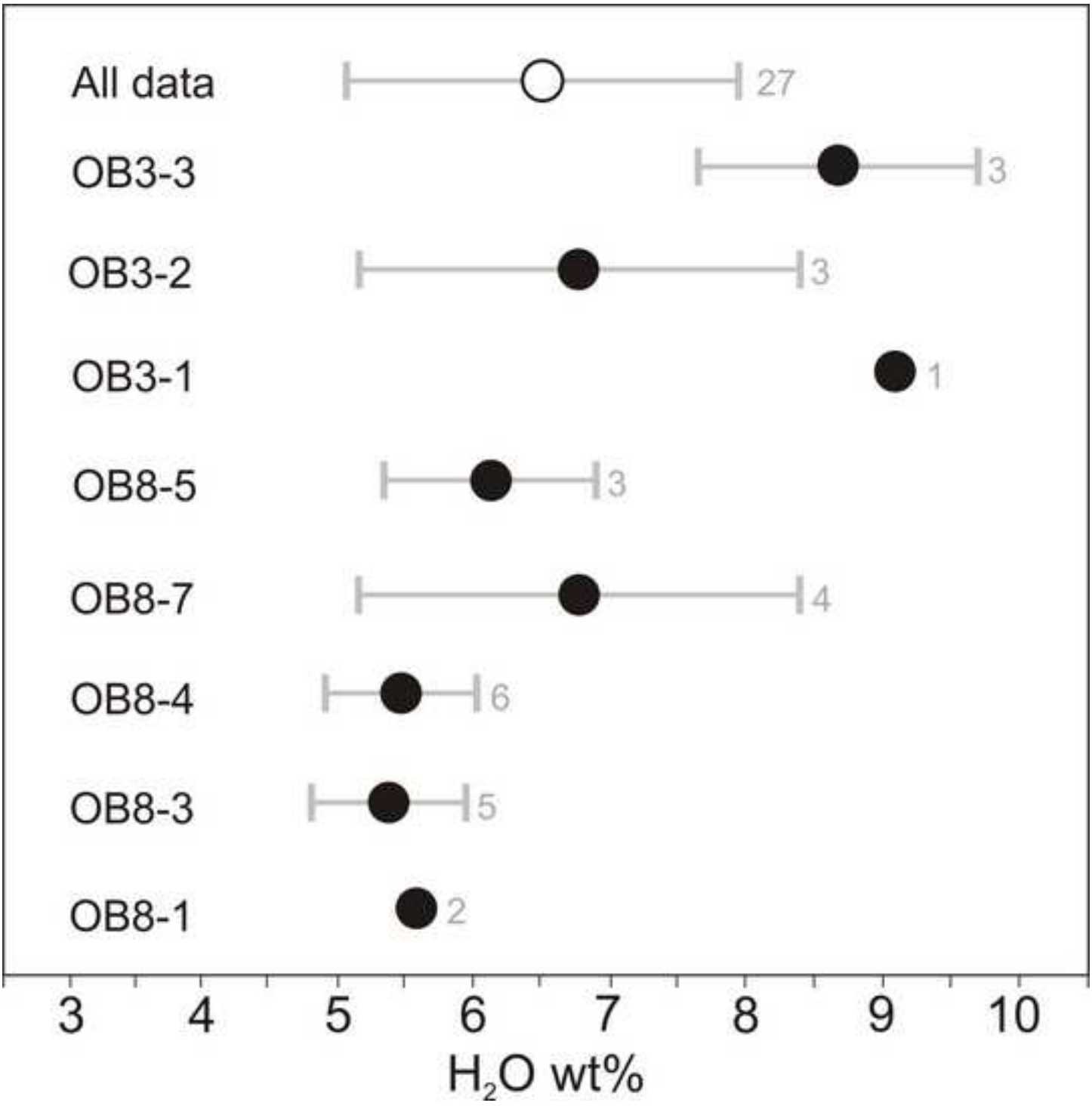

Figure
Click here to download high resolution image

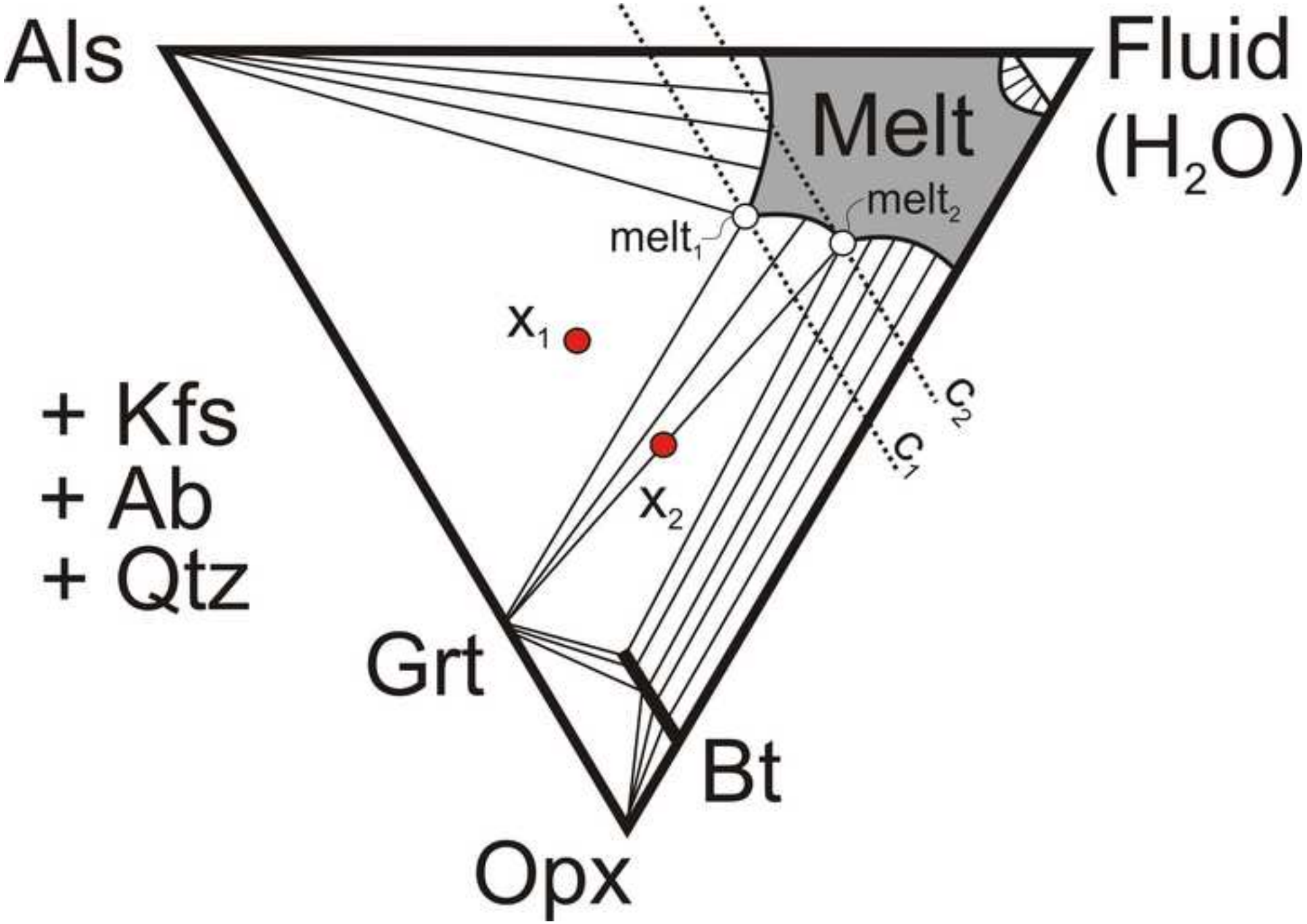

Supplementary material for on-line publication only

Click here to download Supplementary material for on-line publication only: Supporting Online Material.docx